Published in final edited form as:
Chem Soc Rev. 2012 April 7; 41(7): 2673–2685. doi:10.1039/c2cs15229k.

Silica-based nanoprobes for biomedical imaging and theranostic applications†

Juan L. Vivero-Escoto, **Rachel C. Huxford-Phillips**, and **Wenbin Lin**
Department of Chemistry, University of North Carolina at Chapel Hill, CB#390, Chapel Hill, North Carolina 27599, USA. Fax: +1 919-962-2388

Wenbin Lin: wlin@unc.edu

Abstract

Nanoparticle-based contrast agents are attracting a great deal of attention for various biomedical imaging and theranostic applications. Compared to conventional contrast agents, nanoparticles possess several potential advantages to improve *in vivo* detection and to enhance targeting efficiency. Silica-based nanoprobes can be engineered to achieve longer blood circulation times, specific clearance pathways, and multivalent binding. In this *tutorial review,* we summarize the latest progress on designing silica-based nanoprobes for imaging and theranostic applications. The synthesis of both solid silica and mesoporous silica nanoparticles is described, along with different approaches used for surface functionalization. Special emphasis is placed on the application of silica-based nanoprobes in optical, magnetic resonance, and multimodal imaging. The latest breakthroughs in the applications of silica nanoparticles as theranostic agents are also highlighted.

Introduction

Nanomaterials have recently become one of the most active research fields in the areas of engineering, chemistry, solid state physics, biotechnology, and biomedicine. One reason for this interest is that nanomaterials display novel, and often enhanced, properties compared to traditional materials, which opens up the potential for new technological applications. In particular, imaging technologies benefit greatly from using nanomaterials as contrast enhancement agents and molecular probes.[1,2] For example, semiconducting quantum dot (QD) nanoparticles have been a popular option for fluorescent optical imaging due to their broad absorption spectra, narrow and tunable emission spectra, photostability, and high efficiency.[3] Colloidal gold nanoparticles exhibit unique optical and electrical properties (*e.g.* surface plasmon resonance), and can be readily functionalized with biological molecules.[4] As a result, gold nanoparticles have been evaluated for biosensing and as contrast agents for computed tomography (CT). Gold nanoparticles are also being explored for photoacoustic computed tomography (PAT) applications. Superparamagnetic iron oxide nanoparticles (SPIONs) have been used as contrast agents for magnetic resonance imaging (MRI), drug delivery systems, and biosensors.[5] Recently, nanoscale metal–organic frameworks (NMOFs), also known as nanoscale coordination polymers, have been tested for a wide variety of biomedical applications.[6] NMOFs possess many desirable features such as high agent loading, intrinsic biodegradability as a result of labile metal–ligand bonds, high porosity, and versatile functionalization methodologies. NMOFs have been evaluated as novel MRI contrast agents due to their ability to carry large amounts of paramagnetic metal

†Part of the nanomedicine themed issue.

Correspondence to: Wenbin Lin, wlin@unc.edu.

centers and their high per-metal-based relaxivities.[7] They have also been explored for other imaging modalities, such as CT and optical imaging (OI).[8,9]

Interestingly, in contrast to many other nanomaterials, silica nanoparticles do not acquire any special property from their sub-micrometre size, except for the corresponding increase in surface area. What makes silica nanoparticles fascinating from a nanotechnology point of view is their well-defined and tunable structures (*i.e.* size, morphology, and porosity) and surface chemistry. By introducing new functional groups *via* well-established siloxane chemistry, we can modify the silica surface to impart new properties to the particles, such as diagnostic and therapeutic capabilities.[10] Silica nanoparticles are effectively "transparent" in the sense that they do not absorb light in the near-infrared (NIR), visible, and ultraviolet regions or interfere with magnetic fields. In addition, silica nanoparticles are inexpensive, easy to prepare, relatively chemically inert, biocompatible, and water dispersible. This article reviews recent advances in the development of silica nanoparticles as contrast agents for biomedical imaging and theranostic applications.

Synthesis and functionalization of silica nanoparticles

There are two major types of silica-based nanoparticles: solid silica nanoparticles (SiNPs) and mesoporous silica nanoparticles (MSNs). Functionalized SiNPs have been extensively utilized as optical imaging contrast agents and as drug delivery vehicles. As optical contrast agents, SiNPs possess attractive features such as photophysical stability, biocompatibility, and favorable colloidal properties. In addition, the silica surface can be modified by various functional groups such as antibodies, aptamers, and polymers.[11] Typically, two common approaches, the Stöber method and reverse microemulsions, are used to synthesize SiNPs. These methods are based on a sol–gel process in which the hydrolysis of a silicon alkoxide precursor is carried out, followed by the polycondensation of the monomers to afford the desired nanoparticles.

On the other hand, MSNs exhibit many unique properties such as high surface areas, stable and rigid frameworks, tunable pore sizes, and large pore volumes. MSNs are typically synthesized by a surfactant-templated sol–gel approach.[12] MSNs of the MCM-41 structures (MCM stand for Mobil Composition of Matter), for example, possess a honeycomb-like, 2D hexagonal porous structure with empty channels that are able to encapsulate relatively high amounts of functional molecules and shelter them from exposure to the external environment. In addition, these materials have two different surfaces, the interior channel surface and the exterior particle surface, which offer many advantages over solid particles.

Some of the strategies for the synthesis and functionalization of SiNPs and MSNs are described in the following section. More specialized reviews focusing on the synthesis and functionalization of SiNPs[13] and MSNs[14] have recently been published.

Solid silica nanoparticles

The Stöber method and the reverse microemulsion method are generally used to synthesize SiNPs (Fig. 1). The Stöber method, also known as the sol–gel method, was developed by Stöber and coworkers in the late 1960s.[15] The synthesis involves the controlled hydrolysis and condensation of a silica precursor, such as tetraethoxysilane (TEOS), in ethanol and water with ammonia as a catalyst. The size of the particles can be tuned by adjusting the reaction conditions. The nanoparticles obtained by this method are typically monodisperse and spherical in shape. SiNPs remain dispersible in solution due to electrostatic repulsion from their negative surface charges. The Stöber method can also be used to synthesize core–shell nanoparticles when a pre-synthesized core is suspended in the solution.[16]

The reverse microemulsion method was developed by Arriagada and Osseo-Asare in the early 1990s.[17] This approach involves the ammonia-catalyzed polymerization of TEOS in a reverse phase, or water-in-oil, microemulsion. Reverse microemulsions are highly tunable systems that consist of nanometre-sized water droplets stabilized by a surfactant in the organic phase. The micelles of the microemulsion act as "nanoreactors" in which particle growth occurs and the final size is controlled by the water to organic solvent ratio. With this method, highly monodisperse and perfectly spherical particles are obtained with sizes ranging from 20 to 100 nm. The reverse microemulsion method is ideal for producing monodisperse silica nanoparticles smaller than 100 nm.

SiNPs can be functionalized by the addition of hydrophilic functional molecules, which allows for incorporation of organic species within the silica matrix. In this case, functional molecules are entrapped in the silica framework *via* noncovalent interactions. For example, fluorophores such as the tris(2,2′-bipyridyl)dichlororuthenium(II) complex $(Ru(bpy_3))^{2+}$ can be doped into the nanoparticles during the synthesis to impart luminescent properties.[18] Interestingly, entrapped luminophores exhibit a higher quantum yield and enhanced photostability than the free dye molecules. The entrapped dye molecules can leach from the nanoparticles under certain conditions. Functional molecules can also be integrated within the matrix by using organoalkoxysilane derivatives.[11] In this way, small molecules are chemically incorporated within the nanoparticle *via* siloxane linkages, leading to stable hybrid silica nanoparticles with uniform functionalization throughout the nanoparticle and protected from the environment. Entrapped molecules also ameliorate their detrimental intrinsic properties. For example, the release rate of drug molecules can be controlled once loaded inside the silica matrix, and toxicities of QDs and metal nanoparticles are suppressed under the protection of silica shells. Surface functionalization can be achieved by reacting preformed silica nanoparticles with trialkoxysilane derivatives after the nanoparticle synthesis. Post-synthetic grafting is particularly useful for modifying the particle surface with selected agents that are not stable during the silica particle synthesis. In addition, the ability to synthesize nanoparticles with core–shell architectures allows multiple functions to be incorporated within a single platform. For example, gold, QDs, and SPIONs have been embedded into silica nanoparticles to impart catalytic, imaging, and biological capabilities.[19]

Mesoporous silica nanoparticles

Several adjustments to the traditional Stöber method have been reported for the preparation of silica nanoparticles. For example, mesoporous silica particles (MSNs) were prepared by modifying the conditions of the original sol–gel method in the presence of high concentrations of surfactant molecules. The synthesis of MSNs occurs by the formation of liquid-crystalline mesophases of amphiphilic surfactants that function as templates for the polymerization of silica precursors (Fig. 2). The synthesis can be carried out in either acidic or basic conditions. The first reported material, MCM-41, was micrometre-sized particles without a well-defined shape containing hexagonally-ordered channels. Recently, several methods have been developed to control the morphology, pore size, and surface functionalization of MSNs.[12,20] These methodologies have afforded MSNs with different morphologies such as spheres, rods, twisted columns, and kidney bean-shaped nanoparticles. MSNs with particle diameters ranging from 60 to 1000 nm have been synthesized using these methods.

MSNs can be chemically functionalized by two approaches: post-synthetic grafting or co-condensation (Fig. 3). Post-synthetic grafting is the most popular approach for covalently incorporating organic functionalities onto the mesoporous material. This method is based on a condensation reaction between a given trialkoxysilane and the free silanol and geminal silanol groups on the silica surface. This method allows the particle morphology and pore

structure to remain intact, but it has been found that most materials functionalized using this grafting method contain an inhomogeneous coverage of organic functional groups. Using this approach, stimuli-responsive capped MSNs have been synthesized for drug delivery.[21]

Alternatively, MSNs can be functionalized *via* the co-condensation method. In this approach, the desired trialkoxysilane is condensed into the pores of MSNs during the nanoparticle synthesis, leading to homogeneous incorporation of the functional group throughout the material.[12] The selection of the trialkoxysilane precursor is limited to those with organic functional groups that would be soluble in water and can tolerate the extreme pH conditions that are required for the synthesis of MSNs and subsequent removal of surfactants. The degree of functionalization, particle size, and morphology can be modified by adjusting the synthetic conditions, such as reagent concentration and the hydrophobicity/hydrophilicity of the trialkoxysilane reagents. The combination of both synthetic approaches has afforded multifunctional platforms with a wide variety of applications in biotechnology and biomedicine.[20,21]

Biomedical imaging applications of silica nanoparticles

Noninvasive imaging techniques are valuable tools in the arsenal of clinical diagnostics. A diverse range of imaging modalities is now available, from techniques that enable whole-organism anatomical imaging such as MRI and CT, to others that provide specific molecular imaging such as positron electron tomography (PET) and optical fluorescence. Several nanoparticle-based contrast agents have been developed to overcome issues that plague conventional contrast agents. Some of the most important prerequisites for designing nanoparticle-based contrast agents are outlined below:

- Form stable colloidal solutions in a wide variety of *in vitro* and *in vivo* environments
- Possess chemical stability under a wide variety of physiological conditions (*i.e.* solvent polarity, reducing environment, ionic strength, pH, or temperature)
- Exhibit limited nonspecific binding to avoid macrophagocytic system (MPS) uptake
- Have programmed clearance mechanisms
- Display high sensitivity and selectivity for the target (*i.e.,* antigen, cell, or tissue)
- Show good image contrast (high signal-to-noise ratio)
- Have sufficiently long circulation time in the blood if administered intravenously

Ideally, these nanomaterials will be suitable for long-term quantitative imaging at low doses and be safely cleared from the body after imaging is complete. Nanoparticulate silica-based contrast agents are a promising platform to meet the aforementioned requirements.

Silica-based imaging nanoprobes are most commonly used for OI, MRI, or a combination of both modalities. OI is a low cost technology and allows for rapid screening, whereas MRI can offer high resolution and the capacity to simultaneously obtain physiological and anatomical information.

OI is a powerful modality in which specific probes are excited by incident light, usually in the visible or NIR regions, and emit light at a lower energy than the incident light. As radiation is scattered and absorbed quickly within the body, the resolution for OI is limited to 1–2 mm. The need for deeper penetration depths for most clinical applications is driving optical techniques into the NIR region (650–950 nm). OI is a versatile imaging technique in

terms of availability of a variety of contrast agents, avoidance of radiopharmaceuticals, and relatively low cost of instrumentation. These features make OI complementary to other modalities such as MRI and PET.

MRI is currently one of the most powerful *in vivo* imaging technologies, with the advantage of being a noninvasive diagnostic tool that provides high resolution three-dimensional anatomical images of soft tissue. MRI exploits the remarkable range of the physical and chemical properties of water protons.[22,23] The signal detected in MRI results from a combination of total water signal (proton density) and the magnetic properties of the tissues. The magnetic properties in question are the longitudinal relaxation time, T_1, and the transverse relaxation time, T_2. The reciprocals of these values represent the longitudinal and transverse relaxivities, r_1 and r_2, respectively. T_1 and T_2 times are dependent upon the physicochemical environment of a given tissue and are modified in the presence of a pathological state. Contrast enhancement agents are used in imaging to increase the signal difference between the area of interest and the background. In MRI, the sensitivity and exceptional soft tissue contrast are further improved by the use of MR contrast agents that alter the local MR signal intensity. There are two main classes of contrast agents for MRI: paramagnetic complexes and superparamagnetic iron oxide particles. The former class includes mainly chelates of Mn(II), Mn(III), and Gd(III) ions, with Gd-based agents being the most common. The Gd contrast agents currently available lack sensitivity and, thus, high concentrations of contrast agent are required. The use of a nanoparticle platform provides several advantages over small molecule contrast agents. For example, a high payload of a molecular contrast agent can be incorporated within a single nanoparticle, thus increasing the effective relaxivity per nanoparticle. The increased size results in reduced tumbling rates, which increases the relaxivity on a per metal basis.

Solid silica nanoparticles

Many studies incorporating dye molecules into SiNPs for OI have been published. Dye-doped SiNPs were first synthesized by Van Blaaderen and coworkers using the Stöber method with the conjugation of fluorescein isothiocyanate (FITC) with (3-aminopropyl)trimethoxysilane.[24] However, the particles obtained by this method were polydisperse and large (particle diameter of >400 nm). Santra and coworkers synthesized FITC-doped SiNPs in reverse microemulsions,[25] which were further modified with the TAT peptide, a cell-penetrating peptide. To demonstrate biolabeling efficiency, the authors labeled A549 human non-small cell lung cancer and SCC-9 human squamous adenocarcinoma cells *in vitro*. The *in vivo* bioimaging capability of this platform was demonstrated by selectively labelling brain blood vessels *via* intra-arterial administration through the right common carotid artery of a rat. The authors showed that by using TAT-coated SiNPs, it is possible to deliver diagnostic agents to the brain without compromising the blood brain barrier (BBB).

Luminescent metal complexes such as $Ru(bpy)_3^{2+}$ have also been incorporated into SiNPs for OI. The large Stokes shift of this complex significantly reduces the background signal from biological systems. Additionally, $Ru(bpy)_3^{2+}$ is much more photostable than organic fluorophores such as fluorescein. In 2001, Tan and coworkers reported the synthesis of $Ru(bpy)_3^{2+}$-doped SiNPs by the reverse microemulsion method, yielding monodisperse, spherical nanoparticles 63 nm in diameter.[26] This platform exhibited several advantages over small-molecule dyes, such as enhanced signals, increased photostability, homogenous fluorophore distribution, and protection from the external environment. These particles were used as biomarkers by conjugation with an antibody specific for leukemia cells. The leukemia cells were identified easily, concisely, and with high efficiency using the antibody-coated SiNPs. The authors further optimized the reverse microemulsion synthesis of the $Ru(bpy)_3^{2+}$-doped SiNP platform. By changing parameters such as TEOS and ammonium

hydroxide concentrations, type of surfactant, and the molar ratios of water to surfactant and cosurfactant to surfactant, the authors were able to investigate the effects on the fluorescence spectra, particle size, and size distribution of $Ru(bpy)_3^{2+}$-doped SiNPs.[18] Tan and coworkers recently reported findings on the *in vivo* behavior of these nanoparticles.[27] The authors investigated the biodistribution and urinary excretion of three types of surface-modified $Ru(bpy)_3^{2+}$-doped SiNPs (OH–SiNPs, COOH–SiNPs, and PEG–SiNPs) *via* an OI method (PEG = poly(ethylene glycol). PEG is widely used to enhance the biocompatibility and blood circulation time by preventing the nonspecific adsorption of proteins. Results for these *in vivo* imaging studies showed that PEGylated $Ru(bpy)_3^{2+}$-doped SiNPs exhibited longer blood circulation times ($t_{1/2}$ = 180 ± 40 min) and minimal MPS organ uptake than OH–SiNPs and COOH–SiNPs (Fig. 4). Interestingly, *in vivo* real-time imaging showed that all three types of intravenously-injected SiNPs with a size of approximately 45 nm were partially excreted through the renal excretion route; *ex vivo* analysis of organs and urine confirmed these results.

Wiesner and coworkers synthesized highly fluorescent SiNPs by a modified Stöber method.[28] The organic dye (tetramethylrhodamine isothiocyanate, TRITC) was first covalently conjugated to a silica precursor to form a dye-rich core, and silica monomers were subsequently added to afford the core–shell fluorescent SiNPs, referred to as Cornell dots (C dots). These 20–30 nm particles were ~20 times brighter than the constituent dye. The bioimaging utility of these nanoparticles was demonstrated by labelling rat basophilic leukemia mast cells. A thorough investigation of the toxicity and biodistribution of C dots was carried out by Nikitin, Wiesner, and coworkers.[29] No apparent toxicity in the mice was observed. Multiphoton microscopy was used to demonstrate the capability of C dots in sentinel lymph node mapping. C dots can be surface-modified to expand their scope of application. For instance, Langer and coworkers electrostatically coated C dots with cationic polymers to change their surface charge, enabling the particles to escape from the endosomes and enter the cytoplasm and nucleus. Using this strategy, the cellular uptake increased; and these nanoparticles were used as DNA delivery carriers.[30]

The synthesis of C dots was further modified to allow the incorporation of NIR dyes, surface functionalization to avoid opsonization, and multimodal imaging capabilities. Wiesner, Bradbury, and coworkers recently reported the synthesis of NIR C dots with hydrodynamic diameters of 3.3 and 6.0 nm.[31] These nanoparticles contained the NIR dye molecule Cy5 (λ_{em} > 650 nm) and displayed improved photophysical characteristics compared to the parent dye. Biodistribution studies in mice showed that these nanoparticles are partially excreted through the renal pathway; however, significant accumulation in the liver was observed. Further surface modification with PEG (0.5 kDa) showed increased renal excretion and decreased liver uptake compared to the unmodified particles (Fig. 5). The larger 6.0 nm particles exhibited a longer blood circulation time, longer urine half-life, and greater organ retention. Recently, Bradbury and coworkers further modified C dots to afford the next generation of these nanoparticles. This material was designed considering the following features: tumor selectivity, nontoxicity, enhanced targeting, and favorable clearance profiles.[32] These 7 nm particles were synthesized as described above and further functionalized with the cyclic RGD peptide, a target for the $\alpha_v\beta_3$ integrin which is overexpressed in a number of malignant endothelial cell lines, and labeled with the radionuclide ^{124}I. These modified C dots exhibited high-affinity binding *in vitro*, favorable tumor-to-blood residence time ratios, and enhanced tumor-selective accumulation in $\alpha_v\beta_3$ integrin-expressing melanoma xenografts in mice (Fig. 6). In addition, this platform showed high sensitivity, real-time detection and imaging of lymphatic drainage patterns, favorable particle clearance rates, and differential tumor burden in a large animal model (miniswine). This multimodal optical-PET imaging system has recently received FDA approval for a first-in-human clinical trial as a cancer-specific optical probe.[32]

Other approaches have also been explored to develop silica-based OI contrast agents for biomedical applications. Prasad and coworkers reported on the use of multimodal organically-modified silica (ORMOSIL) nanoparticles for *in vivo* bioimaging.[33] These 20–25 nm particles, synthesized using a modified Stöber method, contained a near-IR fluorophore molecule (DY776), and a radio-nuclei ^{124}I label for optical and PET imaging *in vivo*. The authors studied the biodistribution, clearance, and toxicity of these multimodal nanoparticles. The biodistribution of non-targeted nanoparticles was studied in nontumored mice by optical and PET imaging. These studies showed a greater accumulation of nanoparticles in the liver, spleen, and stomach than in the kidneys, heart, and lungs. The clearance studies carried out over a period of 15 days indicated hepatobiliary excretion of the nanoparticles. No apparent toxicity in the mice was observed.

The use of the two-photon absorption approach to overcome the issue of poor depth penetration in OI has attracted a great deal of attention in recent years. Belfield and coworkers synthesized SiNPs containing a two-photon absorbing and aggregation-enhanced NIR-emitting pyran derivative.[34] These particles were surface-modified with PEG and folic acid (FA) to endow targeting capabilities to the nanoprobe. In addition, this platform can be used for two-photon fluorescence microscopy, a well-known technique which provides three-dimensional (3D) cellular-level resolution. These particles were 20–30 nm in size and exhibited a 3-fold increase in two-photon absorption and improved stability over the constituent dye. No apparent toxicity was observed either *in vitro* or *in vivo*. The efficient targeting ability of these SiNPs was demonstrated by intravenous injection into mice bearing HeLa tumors. The nanoprobe not only targeted the tumor, but also penetrated deeply into the tumor parenchyma, as demonstrated by *ex vivo* cellular-level two-photon fluorescence microscopy imaging of the tumor.

The Lin group has focused on the development of multimodal imaging probes combining the MRI and OI modalities. The synthesized 37 nm SiNPs contain an embedded $Ru(bpy)_3^{2+}$ fluorophore and a shell of Gd–DTPA (DTPA = diethylene-triaminepentaacetate) chelates.[35] The surface-immobilized Gd chelates possess relaxivities four orders of magnitude higher than the parent Gd complex, presumably due to Gd chelates attached to the nanoparticles efficiently relaxing water protons through a reduction in the tumbling rates. The Gd chelates were also immobilized on the surface of SiNPs in a multilayer fashion by using a bis(trialkoxysilyl) derivative of Gd–DTPA. However, the SiNPs prepared by this approach exhibited reduced relaxivities on a per Gd basis compared with the monolayer system, likely caused by reduced water accessibility of the Gd chelates.

The efficiency of these SiNPs as a multimodal *in vitro* imaging agent was tested using murine monocyte cells. The monocytes were efficiently labelled, as indicated by flow cytometry results and phantom MR image studies using a 3 T scanner (Fig. 7). This platform can be used for target-specific MR imaging of inflammation by selective trafficking of labelled monocyte cells, as demonstrated by OI and MR imaging using a collagen-induced arthritis (CIA) mouse model.[36] DBA-1J mice were immunized for CIA and imaged after the disease onset. Optical images of the paws were obtained using an optical scanner with filters specific for the spectrum of the $Ru(bpy)_3^{2+}$ fluorophore (excitation: 445–490 nm, emission: 575–650 nm) (Fig. 8). The luminescence intensity correlated well with the clinical disease index and paw swelling in animals that received the SiNP contrast agent, and the strength of this correlation was dose dependent. The post-contrast MR images displayed a 33–55% T_2 reduction when compared to the precontrast images (Fig. 9), corroborating the OI results. Additionally, histopathologic tissue sections of arthritic paws were evaluated with light and fluorescent microscopy to visualize the SiNPs within the hindlimbs. This analysis demonstrated that the particles were located within the synovial tissue where the disease was prevalent.

The Lin group has also developed a polyelectrolyte layer-by-layer (LbL) self-assembly approach for the synthesis of cancer-specific SiNPs with multimodal imaging capabilities.[37] The platform was based on SiNPs containing a $Ru(bpy)_3^{2+}$ core and a monolayer of a negatively-charged Gd–DTPA derivative. This highly anionic nanoparticle was coated with positively-charged Gd chelate oligomers. The resulting positively-charged particle was further treated with negatively-charged polystyrenesulfonate to provide a net negatively-charged layer. These steps were repeated to form the LbL multilayer architecture (Fig. 10). The formation of the LbL SiNPs was confirmed by TEM and fluorescence studies. MR measurements with a 3 T scanner showed that nanoparticles containing the positively-charged Gd chelate (Gd-DOTA) had higher relaxivities on a per Gd basis than the constituent paramagnetic center. Additionally, the LbL self-assembly increases the Gd payload, thus, higher relaxivities on a per particle basis were obtained. To endow targeting abilities to this platform, the K_7RGD targeting group was absorbed on the negatively-charged particles *via* electrostatic interactions. *In vitro* optical and MR imaging studies demonstrated efficient targeting to HT-29 human colon adenocarcinoma cells by the LbL SiNPs with the noncovalently-attached K_7RGD peptide (Fig. 11).

Core–shell nanostructures have been used to incorporate Gd chelates onto QDs, SPIONs, or gold nanoparticles.[38,39] The cores of these nanoparticles provided optical and T_2-weighted contrast, whereas Gd chelates on the surface rendered T_1-weighted MRI enhancements. The biodistribution and blood circulation of these nanoparticles were studied. By functionalizing the surface of NMOF@silica particles with lanthanide chelates, luminescent spore detectors have been developed.[40] In addition, NMOFs with silica shells have been explored for optical, MR imaging, and biosensing applications.[9,41,42]

Mesoporous silica nanoparticles

Dye molecules have been incorporated into the silica framework of MSNs as a tool for investigating cellular internalization and cell tracking.[21] For example, Lindén and coworkers synthesized MSNs for the delivery of imaging agents to cancer cells.[43] The MSN material was first surface-functionalized with poly(ethylene imine). The nanoparticles were then labelled with FITC and modified with FA to endow the targeting ability. *In vitro* experiments using HeLa cells showed that the folate-targeted particles were internalized in a higher amount (5-fold) than the nontargeted nanoparticles. As mentioned previously, OI usually suffers from the attenuation of photon propagation in living tissue and poor signal to noise ratio due to tissue autofluorescence. To overcome these issues, Lo and coworkers developed NIR MSN-based probes.[44] Indocyanine green (ICG) was entrapped into MSNs by electrostatic interactions. ICG is advantageous as a fluorophore for *in vivo* imaging as the dye molecule has been approved by the FDA as an optical contrast agent for clinical applications and its characteristic fluorescent excitation and emission wavelengths ($\lambda_{ex}/\lambda_{em}$ = 800/820 nm) are in the NIR window. The authors demonstrated some of the benefits of using MSNs as scaffolds for incorporating optical agents. For example, the homogeneous dispersion of ICG molecules in the large surface area of MSNs efficiently prevents their aggregation and self-quenching. Moreover, MSNs protect ICG molecules from degradation and diminish the associated immune response. The authors evaluated the biodistribution of this optical probe in rat and mouse models. Optical images revealed that after intravenous injection, the nanoparticles immediately accumulated in liver, followed by the kidneys, lungs, spleen, and heart (Fig. 12). Recently, Lo and coworkers studied the influence of surface charge on the biodistribution of ICG–MSNs.[45] The results showed that by judiciously tailoring the surface charge of MSNs, it is possible to control both biodistribution and the rate of excretion.

The Lin group demonstrated the use of MSNs as nanoparticulate T_1-weighted MR contrast agents *in vitro* and *in vivo*.[46] The nanoprobe was synthesized *via* post-synthetic grafting of a

silane derivative, Gd-Si-DTTA, by refluxing the material in toluene. The MR properties were characterized by 3 T and 9.4 T MR scanners; the nanoparticles exhibited very large r_1 and r_2 relaxivities. The material was labelled with the fluorophore rhodamine B in order to study the *in vitro* properties using an immortalized murine monocyte cell line. Both confocal microscopy and *in vitro* phantom images showed that the nanoparticles were internalized by the monocytes.

The MSN material was intravenously injected to a mouse to study the *in vivo* MR contrast enhancement properties. T_1-weighted contrast enhancement was clearly visible in the aorta of the mouse 15 min post-injection. This enhancement shows the potential of the Gd–MSN platform as an intravascular MR contrast agent (Fig. 13). Moreover, it was also demonstrated that when administered in higher doses, this nanoprobe can be used as a T_2-weighted contrast agent. Signal loss was observed in the liver several days after administration of the Gd–MSN material. The slow excretion of the Gd–MSN nanoprobe after the MRI study, as well as consequent long-term tissue accumulation of toxic Gd^{3+} ions, could result in potential toxicological issues. Recently, the Lin group synthesized a multifunctional MSN-based MRI contrast agent that can be quickly excreted by the renal pathway after imaging.[47] This nanoprobe contains a Gd-chelate unit that is covalently bound to MSN *via* a redox-responsive linker. The MSN-based MR imaging platform was further functionalized with PEG and an anisamide ligand to improve its biocompatibility and target specificity. Anisamide is known to target sigma receptors, which are overexpressed in a number of epithelial cancer cell types. The effectiveness of this nanoprobe and its targeting ability were successfully demonstrated *in vitro* using human colon adenocarcinoma and pancreatic cancer cells. Finally, the biodegradability and capability of this platform as an *in vivo* MR contrast agent was evaluated using a 3 T scanner. The Gd chelate unit was quickly cleaved by the blood pool thiols and the Gd complex was rapidly eliminated *via* the renal excretion pathway.

The ability to monitor cell trafficking and biodistribution *in vivo* is a prerequisite for developing successful stem cell therapies. MR is an ideal noninvasive imaging technique for tracking stem cells; however, cells must be magnetically labelled by endocytic internalization. Hence, more efficient noninvasive cellular-internalizing platforms are highly desirable. Huang, Mou, and coworkers have used silica nanoparticles as multimodal contrast agents for tracking stem cells.[48,49] The MSN-based dual-modal platform combines a fluorescent dye (FITC) and a MR contrast agent. Both T_2- and T_1-weighted MR contrast agents have been incorporated into this system. Small particles of iron oxide behave as negative contrast agents to afford Mag-Dye@MSNs,[49] and Gd-based chelates were grafted onto MSNs to afford Gd-Dye@MSNs.[48] Both systems were efficiently internalized into human mesenchymal stem cells (hMSCs) without affecting cell viability, growth, or differentiation. The efficient hMSCs tracking was visualized *in vitro* and *in vivo* by a clinical 1.5 T MRI system. *In vivo*, the labeled cells remained detectable by MRI after long-term growth or differentiation, providing further evidence of the biocompatibility and durability of both of the Mag-Dye and Gd-Dye@MSNs nanoprobes (Fig. 14). In addition, Mou and coworkers used the dual-modality Mag-Dye@MSNs system to follow the biodistribution of MSNs *in vivo* after eye vein injection in a mouse model.[49] T_2-weighted MR images revealed that the MSNs started to accumulate immediately in the liver, spleen, and kidneys predominantly through a vascular mechanism, and signal darkening was observed mainly in the liver and spleen due to nanoparticle accumulation within the RES at later time points post injection. To confirm these results, histology slides prepared from the above-mentioned organs of mice sacrificed 30 min after administration of Mag-Dye@MSNs were visualized by a fluorescence microscope. Fluorescence due to FITC was observed in the liver and spleen, but not in the kidneys. A long-term MRI tracking study in the liver

showed that the Mag-Dye@MSNs are highly resistant to decomposition and not easily excreted from the body.

Simultaneous imaging and therapeutic applications of silica nanoparticles

In recent years, there has been a remarkable level of research interest in using multifunctional nanomaterials for simultaneous imaging and therapy. The field has expanded so rapidly that the term “theranostic” (syn: theragnostic) has been coined to describe platforms that serve dual roles as diagnostic and therapeutic agents.[50] The inspiration for this approach is that theranostic agents could provide the ability to simultaneously monitor the disease, the therapeutic agent uptake, and the efficacy of the treatment. One of the advantages of nanomaterials is that many of them are already imaging agents (QDs, SPIONs, C dots, and Au nanoparticles) and can be readily “upgraded” to theranostic agents by incorporating therapeutic functions on these platforms. In addition, an underlying driving force of such a combination is that imaging and therapy both require sufficient accumulation of agents in diseased areas. Silica nanoparticles are an excellent scaffold for facile loading of a wide variety of imaging and therapeutic moieties, making them promising candidates for theranostic applications. This section describes some of the most illustrative examples of silica-based theranostic nanoparticles.

Solid silica nanoparticles

SiNPs have been recently used for photodynamic therapy (PDT) applications. PDT is a localized treatment that destroys targeted cells with reactive oxygen species (ROS), such as single oxygen ($^1O_2$), that are generated by irradiating a photosensitizer in the presence of oxygen. PDT is particularly attractive because it combines two essentially harmless elements (a photosensitizer and light) to produce singlet oxygen, which is known to be destructive to cancer cells.[51] In addition, the function of photosensitizers is not restricted solely to the therapeutic generation of singlet oxygen. Many photosensitizers function as bright fluorophores, and some of them emit in the NIR region of the spectra, which is preferred for *in vivo* OI. Nanoparticle carrying photosensitizers can be used as theranostic agents for PDT. Prasad and coworkers described the use of the ORMOSIL material for PDT.[52] The authors incorporated 2-devinyl-2-(1-hexyloxyethyl)pyropheophorbide (HPPH), a hydrophobic photosensitizer, into silica matrices. It was demonstrated that HPPH is more fluorescent in the silica matrices than in the free form and can efficiently kill cancer cells when irradiated with a laser. The main drawback of PDT is that currently approved photosensitizers absorb in the visible spectral region, where light penetration depth is only a few millimetres. This problem can be alleviated by using NIR dyes or combining a two-photon absorbing dye with the photosensitizer. Hai and coworkers reported on the preparation of 105 nm silica particles with entrapped methylene blue for OI and PDT.[53] The therapeutic efficacy of this system was demonstrated *in vitro* and *in vivo*.

Both fluorescence imaging and PDT were observed in a mouse xenograft model. After intratumoral injection of the methylene blue-loaded nanoparticles, optical images of the mice showed that the tumor region was clearly defined, and after laser treatment, the tumor became necrotic (Fig. 15). Recently, Prasad and coworkers described the co-encapsulation of HPPH and a two-photon absorbing dye, 9,10-bis[4′-(4″-aminostyryl)styryl]anthracene (BDSA), into silica nanoparticles.[54] It was shown that BDSA can efficiently up-convert the NIR light and partially transfer the energy to HPPH to activate PDT function. NMOF@silica particles have also been developed for theranostic applications; iron-carboxylate MIL-101 particles were post-synthetically modified to introduce both therapeutic and imaging moieties.[55]

Mesoporous silica nanoparticles

MSNs are especially appropriate for the development of theranostic nanoparticles. Due to their unique topology with three different domains—silica matrix, internal, and external surfaces—MSNs can incorporate numerous functional groups, such as contrast agents, therapeutics, and biomolecular targeting ligands. For example, Lo and coworkers developed a MSN-based theranostic platform that was functionalized with three different chemical entities. A NIR dye (ATTO 647N) was co-condensed into the silica framework, and a photosensitizer (*meso*-tetratolylporphyrin-Pd, PdTPP) was grafted within the channels of MSN. Finally, the exterior surface was functionalized with cyclic RGD attached to a PEG chain.[56] The authors evaluated the targeting specificity and uptake of nano-particles by comparing tumor cells that lack the $\alpha_v\beta_3$ integrin (MCF-7 breast cancer) and those that overexpress the $\alpha_v\beta_3$ integrin (U87-MG glioblastoma). The flow cytometry and confocal microscopy data showed that U87-MG cells selectively internalize RGD-PdTPP-MSN particles. PDT efficacy was tested by bioavailability assays under irradiation (532 nm diode laser; 250 ± 5 mW cm^{-2}) and non-irradiation conditions. The results revealed a dramatic difference in post-irradiation cytotoxic response of U87-MG cells that have been treated with RGD-PdTPP-MSN particles.

Brinker and coworkers have developed MSN-supported lipid bilayers (protocells) as a theranostic platform (Fig. 16).[57] By synergistically combining features of MSNs and liposomes, the authors loaded a mixture of therapeutic (drugs, siRNA, and toxins) and diagnostic agents (QDs) and modified this system to promote cell targeting, endosomal escape, and nuclear accumulation of selected cargos.

Recently, Moon, Hyeon, and coworkers synthesized a monodisperse core–shell platform consisting of a single iron oxide (IO) nanocrystal surrounded by a shell of mesoporous silica (IO@MSNs).[58] The size of these particles can easily be controlled below 100 nm. The material was further functionalized with optical agents (FITC and rhodamine B) and PEG chains. The OI capability of this material was used to determine its internalization in MCF-7 breast cancer cells. Moreover, the MR T_2-weighted properties of IO@MSNs-PEG were measured with a 1.5 T scanner. The r_1 and r_2 relaxivity values of the core–shell system were 3.40 and 245 mM^{-1} s^{-1}, respectively. Fluorescent and T_2-weighted phantom MR images showed that the uptake of the particles is concentration dependent. To evaluate IO@MSNs-PEG as a drug delivery vehicle, doxorubicin (DOX), a well-known anti-cancer agent, was loaded, and the therapeutic efficacy of this system was determined using the SK-BR-3 cell line. A cytotoxicity assay demonstrated the efficacy of this nanoparticle in delivering DOX inside SK-BR-3 cells. The authors investigated the *in vivo* imaging abilities of this platform in a breast cancer xenograft model. After 2 h post-injection, the accumulation of nanoparticles in the tumor was detected by T_2-weighted MR. The accumulation of IO@MSNs-PEG was further confirmed by fluorescence imaging of the tumor and organs of mice sacrificed 24 h after injection. Additionally, the authors recently reported the synthesis of dye-doped IO-capped MSNs for multimodal imaging and drug delivery applications.[59] In this approach, the fluorophore (FITC or TRITC) was doped in the channels, and the IO nanoparticles were chemically attached to the exterior surface of MSNs. Similar to the previous study, the nanoparticles were further functionalized with PEG. The T_2-weighted MR properties of this material were characterized by a 1.5 T scanner. Interestingly, the assembly of multiple IO nanoparticles on MSN resulted in a remarkable T_2-weighted MR contrast enhancement; r_2 values for free IO and IO-MSN were 26.8 mM^{-1} s^{-1} and 76.2 mM^{-1} s^{-1}, respectively. The multimodal imaging capabilities of this platform were tested *in vitro*; fluorescence and T_2-weighted MR images demonstrated that IO-MSN can be used as a multimodal probe. DOX was loaded into the particles, and the antitumor efficacy of this vehicle was tested using the B16-F10 melanoma cell line. *In vivo* evaluations were carried out by intravenous injection into nude mice bearing tumors. At 3 h postinjection, the T_2-

weighted MR signal decreased at the tumor site, demonstrating passive targeting of IO-MSNs by the enhanced permeability and retention (EPR) effect. The delivery of DOX to the tumor tissue was demonstrated by fluorescence emitted by DOX accumulated at the tumor site. The antitumor activity of this platform was evaluated using the TUNEL assay (Fig. 17).

Recently, Tamanoi and coworkers reported the synthesis of MSN-based theranostic particles that contain an OI agent (FITC) and an anticancer therapeutic (camptothecin, CPT). In this work, the authors focused on the toxicity, biodistribution, clearance, and therapeutic properties of MSNs.[60] The short- and long-term toxicities of MSNs were studied, and no apparent toxicity in the animal model was observed. The biodistribution and excretion of MSNs were determined by OI and ICP-OES, respectively. Fluorescent images showed that MSN particles are mainly localized in the tumor, kidneys, and liver. Both renal and hepatobiliary routes of excretion were investigated; the results obtained from the urine and feces showed that the material is cleared through both pathways. To evaluate the therapeutic efficacy of CPT-loaded MSNs *in vivo*, a xenograft model of MCF-7 human breast cancer cells was used. The authors observed significant tumor growth inhibition with the theranostic particles at the conclusion of the experiment.

Conclusions

Silica-based contrast agents are promising platforms for biomedical imaging and theranostic applications. These materials can be engineered with numerous functionalities to achieve specific physical and chemical properties. *In vitro*, the advantages of these platforms over small molecule contrast agents have been demonstrated. In addition, recent *in vivo* results have confirmed their promise as diagnostic tools. FDA approval of C dots for the first-in-human clinical trial is an encouraging advance in this field. However, some areas still need to be further investigated before translation into the clinic becomes a reality. These concerns include the biocompatibility, long-term toxicity, targeting efficiency, and biodegradability of silica-based nanoprobes. The present trend in this field is to develop theranostic platforms that incorporate additional functionalities (*i.e.* therapeutic agents) with the *in vivo* imaging modalities, rendering these platforms as theranostics. Interdisciplinary collaborations are critically needed to enable the adoption of silica-based nanoprobes in the clinic as imaging and therapeutic agents.

Acknowledgments

We thank the National Cancer Institute (U01-CA151455 and U54-CA151652) for financial support. J.V.-E. acknowledges the Carolina Postdoctoral Program for Faculty Diversity for a postdoctoral fellowship.

Notes and references

1. Choi HS, Frangioni JV. Mol Imaging. 2010; 9:291–310. [PubMed: 21084027]
2. Cho EC, Glaus C, Chen J, Welch MJ, Xia Y. Trends Mol Med. 2010; 16:561–573. [PubMed: 21074494]
3. Zrazhevskiy P, Sena M, Gao X. Chem Soc Rev. 2010; 39:4326–4354. [PubMed: 20697629]
4. Huang X, Jain PK, El-Sayed IH, El-Sayed MA. Nanomedicine. 2007; 2:681–693. [PubMed: 17976030]
5. Lin W, Hyeon T, Lanza GM, Zhang M, Meade TJ. MRS Bull. 2009; 34:441–448.
6. Della Rocca J, Liu D, Lin W. Acc Chem Res. 2011; 44:957–968. [PubMed: 21648429]
7. Della Rocca J, Lin W. Eur J Inorg Chem. 2010:3725–3734.
8. deKrafft KE, Xie Z, Cao G, Tran S, Ma L, Zhou OZ, Lin W. Angew Chem, Int Ed. 2009; 48:9901–9904.
9. Liu D, Huxford RC, Lin W. Angew Chem, Int Ed. 2011; 50:3696–3700.

10. Taylor-Pashow KML, Della Rocca J, Huxford RC, Lin W. Chem Commun. 2010; 46:5832–5849.
11. Wang L, Zhao W, Tan W. Nano Res. 2008; 1:99–115.
12. Slowing II, Vivero-Escoto JL, Trewyn BG, Lin VSY. J Mater Chem. 2010; 20:7924–7937.
13. Liang S, John CL, Xu S, Chen J, Jin Y, Yuan Q, Tan W, Zhao JX. Springer Ser Fluoresc. 2010; 9:229–251.
14. Trewyn BG, Slowing II, Giri S, Chen HT, Lin VSY. Acc Chem Res. 2007; 40:846–853. [PubMed: 17645305]
15. Stoeber W, Fink A, Bohn E. J Colloid Interface Sci. 1968; 26:62–69.
16. Piao Y, Burns A, Kim J, Wiesner U, Hyeon T. Adv Funct Mater. 2008; 18:3745–3758.
17. Arriagada FJ, Osseo-Asare K. Colloids Surf. 1992; 69:105–115.
18. Bagwe RP, Yang C, Hilliard LR, Tan W. Langmuir. 2004; 20:8336–8342. [PubMed: 15350111]
19. Guerrero-Martinez A, Perez-Juste J, Liz-Marzan LM. Adv Mater. 2010; 22:1182–1195. [PubMed: 20437506]
20. Wu SH, Hung Y, Mou CY. Chem Commun. 2011; 47:9972–9985.
21. Vivero-Escoto JL, Slowing II, Trewyn BG, Lin VSY. Small. 2010; 6:1952–1967. [PubMed: 20690133]
22. Na HB, Song IC, Hyeon T. Adv Mater. 2009; 21:2133–2148.
23. Villaraza AJL, Bumb A, Brechbiel MW. Chem Rev. 2010; 110:2921–2959. [PubMed: 20067234]
24. Van Blaaderen A, Vrij A. Langmuir. 1992; 8:2921–2931.
25. Santra S, Yang H, Dutta D, Stanley JT, Holloway PH, Tan W, Moudgil BM, Mericle RA. Chem Commun. 2004:2810–2811.
26. Santra S, Zhang P, Wang K, Tapec R, Tan W. Anal Chem. 2001; 73:4988–4993. [PubMed: 11681477]
27. He X, Nie H, Wang K, Tan W, Wu X, Zhang P. Anal Chem. 2008; 80:9597–9603. [PubMed: 19007246]
28. Ow H, Larson DR, Srivastava M, Baird BA, Webb WW, Wiesner U. Nano Lett. 2005; 5:113–117. [PubMed: 15792423]
29. Choi J, Burns AA, Williams RM, Zhou Z, Flesken-Nikitin A, Zipfel WR, Wiesner U, Nikitin AY. J Biomed Opt. 2007; 12:064007. [PubMed: 18163823]
30. Fuller JE, Zugates GT, Ferreira LS, Ow HS, Nguyen NN, Wiesner UB, Langer RS. Biomaterials. 2008; 29:1526–1532. [PubMed: 18096220]
31. Burns AA, Vider J, Ow H, Herz E, Penate-Medina O, Baumgart M, Larson SM, Wiesner U, Bradbury M. Nano Lett. 2009; 9:442–448. [PubMed: 19099455]
32. Benezra M, Penate-Medina O, Zanzonico PB, Schaer D, Ow H, Burns A, DeStanchina E, Longo V, Herz E, Iyer S, Wolchok J, Larson SM, Wiesner U, Bradbury MS. J Clin Invest. 2011; 121:2768–2780. [PubMed: 21670497]
33. Kumar R, Roy I, Ohulchanskky TY, Vathy LA, Bergey EJ, Sajjad M, Prasad PN. ACS Nano. 2010; 4:699–708. [PubMed: 20088598]
34. Wang XH, Morales AR, Urakami T, Zhang LF, Bondar MV, Komatsu M, Belfield KD. Bioconjugate Chem. 2011; 22:1438–1450.
35. Rieter WJ, Kim JS, Taylor KML, An H, Lin W, Tarrant T, Lin W. Angew Chem, Int Ed. 2007; 46:3680–3682.
36. Kim JS, An H, Rieter WJ, Esserman D, Taylor-Pashow KML, Sartor RB, Lin W, Tarrant TK. Clin Exp Rheumatol. 2009; 27:580–586. [PubMed: 19772788]
37. Kim JS, Rieter WJ, Taylor KML, An H, Lin W, Lin W. J Am Chem Soc. 2007; 129:8962–8963. [PubMed: 17602632]
38. Huang CC, Tsai CY, Sheu HS, Chuang KY, Su CH, Jeng US, Cheng FY, Su CH, Lei HY, Yeh CS. ACS Nano. 2011; 5:3905–3916. [PubMed: 21513334]
39. van Schooneveld MM, Vucic E, Koole R, Zhou Y, Stocks J, Cormode DP, Tang CY, Gordon RE, Nicolay K, Meijerink A, Fayad ZA, Mulder WJM. Nano Lett. 2008; 8:2517–2525. [PubMed: 18624389]
40. Taylor KML, Lin W, Mater J. Chem. 2009; 19:6418–6422.

41. Taylor KML, Rieter WJ, Lin W. J Am Chem Soc. 2008; 130:14358–14359. [PubMed: 18844356]
42. Rieter WJ, Taylor KML, Lin W. J Am Chem Soc. 2007; 129:9852–9853. [PubMed: 17645339]
43. Rosenholm JM, Peuhu E, Eriksson JE, Sahlgren C, Linden M. Nano Lett. 2009; 9:3308–3311. [PubMed: 19736973]
44. Lee CH, Cheng SH, Wang YJ, Chen YC, Chen NT, Souris J, Chen CT, Mou CY, Yang CS, Lo LW. Adv Funct Mater. 2009; 19:215–222.
45. Souris JS, Lee CH, Cheng SH, Chen CT, Yang CS, Ho J-aA, Mou C-Y, Lo L-W. Biomaterials. 2010; 31:5564–5574. [PubMed: 20417962]
46. Taylor KML, Kim JS, Rieter WJ, An H, Lin W, Lin W. J Am Chem Soc. 2008; 130:2154–2155. [PubMed: 18217764]
47. Vivero-Escoto JL, Taylor-Pashow KML, Huxford RC, Della Rocca J, Okoruwa C, An H, Lin W, Lin W. Small. 2011; 7:3519–3528. [PubMed: 22069305]
48. Hsiao JK, Tsai CP, Chung TH, Hung Y, Yao M, Liu HM, Mou CY, Yang CS, Chen YC, Huang DM. Small. 2008; 4:1445–1452. [PubMed: 18680095]
49. Liu HM, Wu SH, Lu CW, Yao M, Hsiao JK, Hung Y, Lin YS, Mou CY, Yang CS, Huang DM, Chen YC. Small. 2008; 4:619–626. [PubMed: 18491363]
50. Janib SM, Moses AS, MacKay JA. Adv Drug Delivery Rev. 2010; 62:1052–1063.
51. Berg K, Selbo PK, Weyergang A, Dietze A, Prasmickaite L, Bonsted A, Engesaeter BO, Angell-Petersen E, Warloe T, Frandsen N, Hogset A. J Microsc. 2005; 218:133–147. [PubMed: 15857375]
52. Roy I, Ohulchanskyy TY, Pudavar HE, Bergey EJ, Oseroff AR, Morgan J, Dougherty TJ, Prasad PN. J Am Chem Soc. 2003; 125:7860–7865. [PubMed: 12823004]
53. He X, Wu X, Wang K, Shi B, Hai L. Biomaterials. 2009; 30:5601–5609. [PubMed: 19595455]
54. Kim S, Ohulchanskyy TY, Pudavar HE, Pandey RK, Prasad PN. J Am Chem Soc. 2007; 129:2669–2675. [PubMed: 17288423]
55. Taylor-Pashow KML, Della Rocca J, Xie Z, Tran S, Lin W. J Am Chem Soc. 2009; 131:14261–14263. [PubMed: 19807179]
56. Cheng SH, Lee CH, Chen MC, Souris JS, Tseng FG, Yang CS, Mou CY, Chen CT, Lo LW. J Mater Chem. 2010; 20:6149–6157.
57. Ashley CE, Carnes EC, Phillips GK, Padilla D, Durfee PN, Brown PA, Hanna TN, Liu J, Phillips B, Carter MB, Carroll NJ, Jiang X, Dunphy DR, Willman CL, Petsev DN, Evans DG, Parikh AN, Chackerian B, Wharton W, Peabody DS, Brinker CJ. Nat Mater. 2011; 10:389–397. [PubMed: 21499315]
58. Kim J, Kim HS, Lee N, Kim T, Kim H, Yu T, Song IC, Moon WK, Hyeon T. Angew Chem, Int Ed. 2008; 47:8438–8441.
59. Lee JE, Lee N, Kim H, Kim J, Choi SH, Kim JH, Kim T, Song IC, Park SP, Moon WK, Hyeon T. J Am Chem Soc. 2010; 132:552–557. [PubMed: 20017538]
60. Lu J, Liong M, Li Z, Zink JI, Tamanoi F. Small. 2010; 6:1794–1805. [PubMed: 20623530]

Biographies

Juan L. Vivero-Escoto obtained his BSc and MSc in Chemical Engineering from the National Polytechnic Institute of Mexico. He earned his PhD degree from Iowa State University in 2009 under the supervision of late Prof. Victor S.-Y. Lin. Currently he is

working with Prof. Wenbin Lin at the University of North Carolina at Chapel Hill with a postdoctoral fellowship from the Carolina Postdoctoral Program for Faculty Diversity. His current research involves the development of hybrid materials for biomedical applications.

Rachel C. Huxford-Phillips received her BS and MS in chemistry from Tennessee Technological University in 2007 and 2008, respectively. Her MS thesis research was carried out under the supervision of Prof. Edward Lisic. She is currently in the fourth year of pursuing her doctorate degree in chemistry from the University of North Carolina at Chapel Hill under Prof. Wenbin Lin. Her current research focuses on the development of nanoscale coordination polymers for biomedical applications.

Wenbin Lin is the Kenan Distinguished Professor of chemistry and pharmacy at the University of North Carolina at Chapel Hill. His research interests center around designing molecular materials for sustainability and human health, with ongoing research projects on designing framework materials for asymmetric catalysis, solar energy utilization, and heavy metal sequestration and developing hybrid nanomaterials for biomedical imaging and drug delivery. He has published ~185 papers in several research areas.

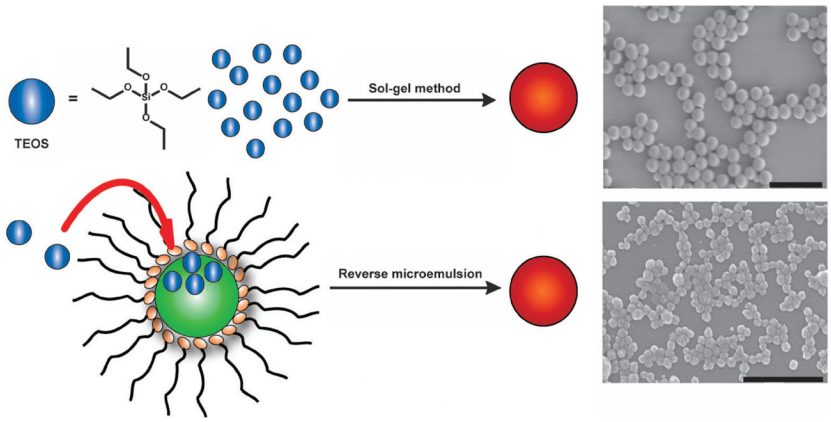

Fig. 1.

Schematic showing the synthesis of SiNPs by the Stöber method (top), in which the hydrolysis and condensation of TEOS is facilitated by the base in ethanol and water, and *via* reverse phase microemulsion (bottom), in which TEOS is hydrolyzed at the micellar interface and enters the aqueous droplet to form a silica nanoparticle. The scale bars represent 1000 nm and 500 nm, respectively.

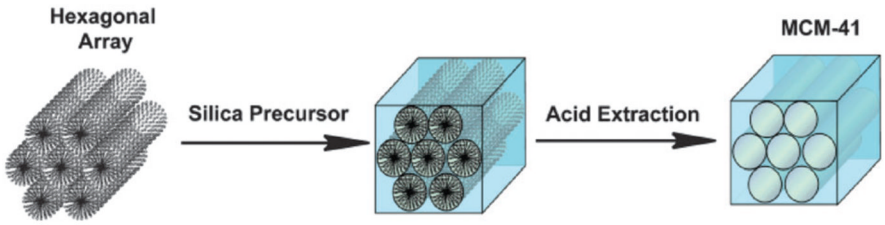

Fig. 2.
Schematic representation of the synthesis of MCM-41 type MSN particles. The cationic surfactant molecules self-assemble into hexagonal arrays in aqueous solution and the silica precursors then hydrolyze and condense along the exterior of the micelles to form a mesoporous material after extraction of the surfactant.

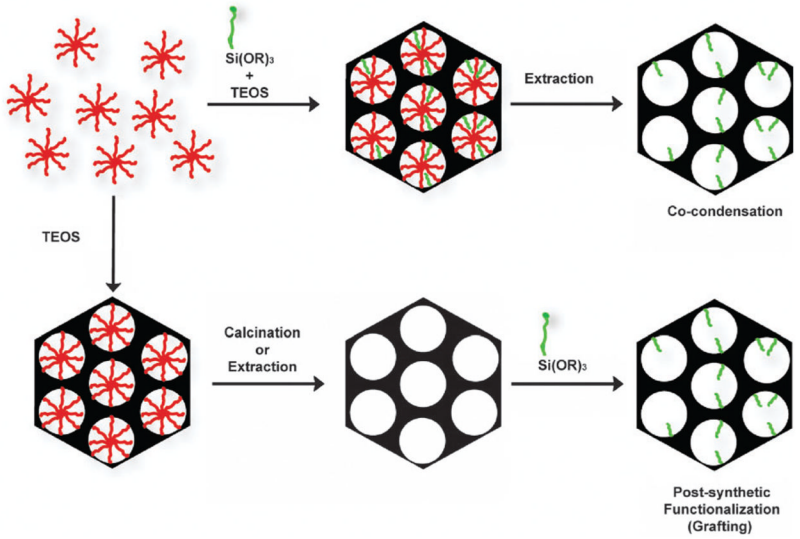

Fig. 3.

Functionalization of MSNs by co-condensation (top) or the post-synthetic method (bottom). A trialkoxysilane molecule bearing a functional group (green) is shown as an example of a silica precursor. The structure-directing agent is represented by micelles (red).

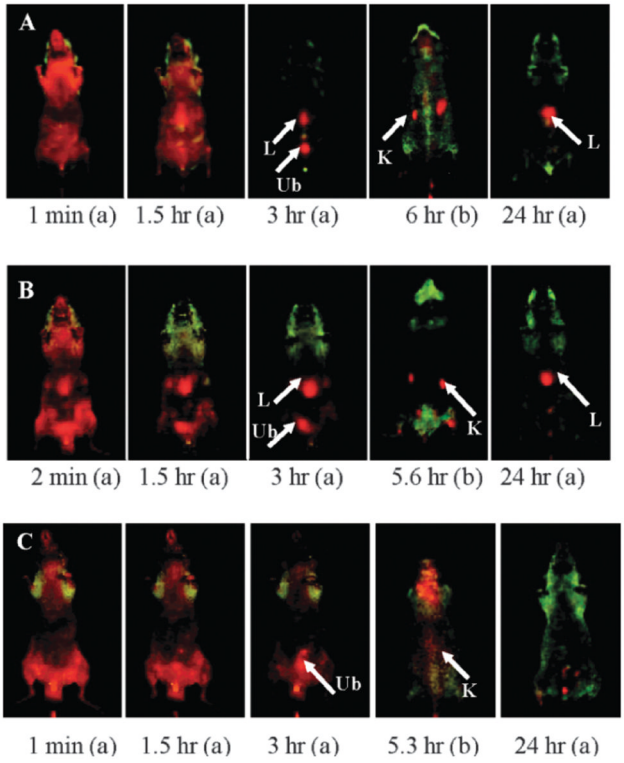

Fig. 4.

In vivo imaging of biodistribution of intravenously-injected surface-modified SiNPs at different time points post-injection: (a) abdomen image and (b) back image. (A) OH–SiNPs, (B) COOH–SiNPs. (C) PEG–SiNPs. Arrows indicate the location of the kidney (K), liver (L), and urinary bladder (Ub). Reprinted from ref. 27 with permission from American Chemical Society.

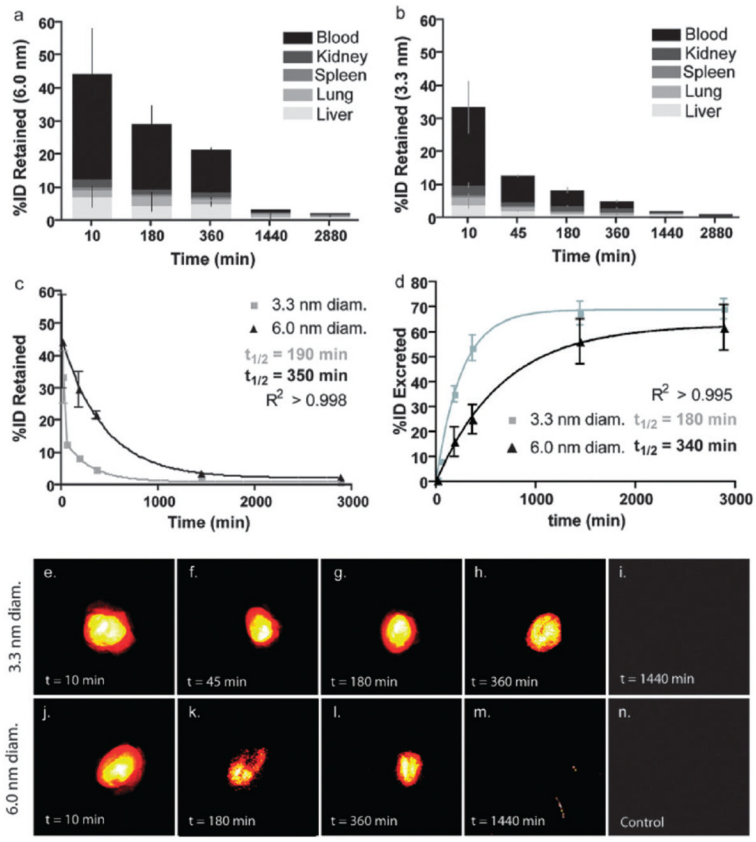

Fig. 5.

Biodistribution analysis of C-dots in mice (top) and fluorescence pseudo-color imaging of a mouse bladder *ex vivo* (bottom). (a, b) Percent of initial particle dose (% ID) retained for 6.0 nm (a) and 3.3 nm (b) diameter C dots. (c) Plot of retained particle concentration for 3.3 nm (light gray) and 6.0 nm (black). (d) Plot of estimated particle excretion for 3.3 nm (light gray) and 6.0 nm (black). (e–i) Pseudocolor images of Cy5 fluorescence in intact mouse bladders showing the accumulation of 3.3 nm (e–h), followed by the negligible particle fluorescence seen at 24 h postinjection (i). (j–m) Pseudocolor images of Cy5 fluorescence in intact mouse bladders showing the accumulation of 6.0 nm (j–l) and at the 24 h end point (m). (n) Pseudocolor image of a control mouse bladder. Reprinted from ref. 31 with permission from American Chemical Society.

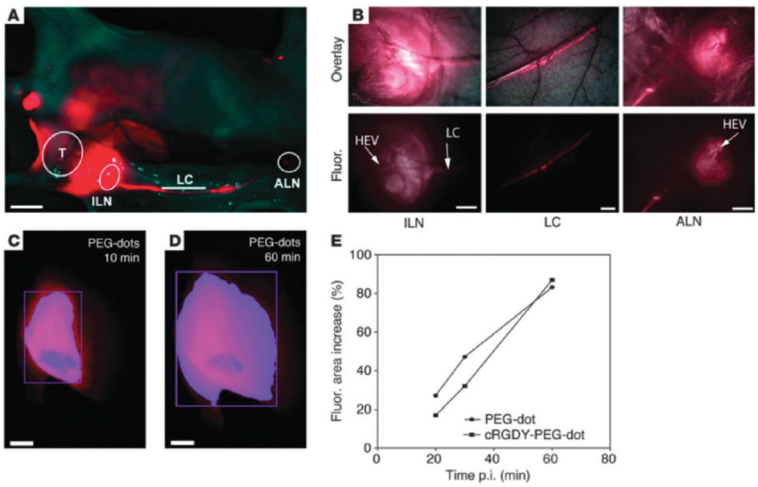

Fig. 6.

Nodal mapping using multiscale NIR optical fluorescence imaging. (A) Whole-body fluorescence imaging of the tumor site (T), draining inguinal (ILN) and axillary (ALN) nodes, and communicating lymphatic channels (LCs). (B) Corresponding coregistered white-light and high-resolution fluorescence images (top row) and fluorescence images only (bottom row), revealing the nodal infrastructure of local and distant nodes, including high endothelial venules (HEVs). (C) Whole-body fluorescence image of the tumor site 10 minutes after sub-dermal PEG-dot injection. (D) Delayed whole-body fluorescence image of the tumor site 1 h after PEG-dot injection. (E) Percent increase in the area of fluorescence (fluor) relative to that measured at 10 min post-injection for targeted and nontargeted probes. Scale bars: 1.0 cm (A); 500 μm (B); 3 mm (C and D). Reprinted from ref. 32 with permission from American Society for Clinical Investigation.

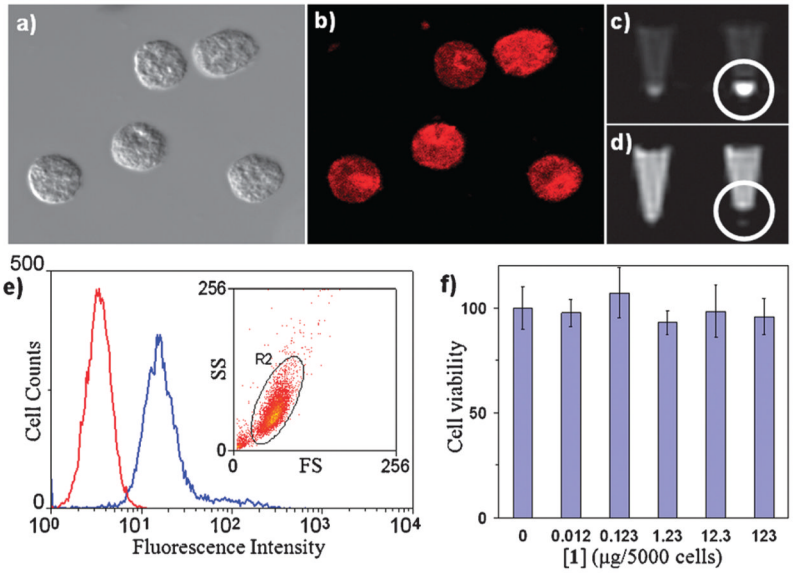

Fig. 7.

Microscopic images of labeled monocyte cells: (a) optical image and (b) laser scanning confocal fluorescence. (c, d) MR images of unlabeled (left) and labeled (right) monocyte cells: (c) T_1-weighted and (d) T_2-weighted. (e) Flow cytometry results for the unlabeled (red) and labeled (blue) monocyte cells indicating greater than 98% labeling efficiency (inset shows the purity of the labeled cells; SS = side scatter, FS = forward scatter). (f) MTS assay of the monocyte cells incubated with different amounts of nanoparticles. Reprinted from ref. 35 with permission from John Wiley & Sons Inc.

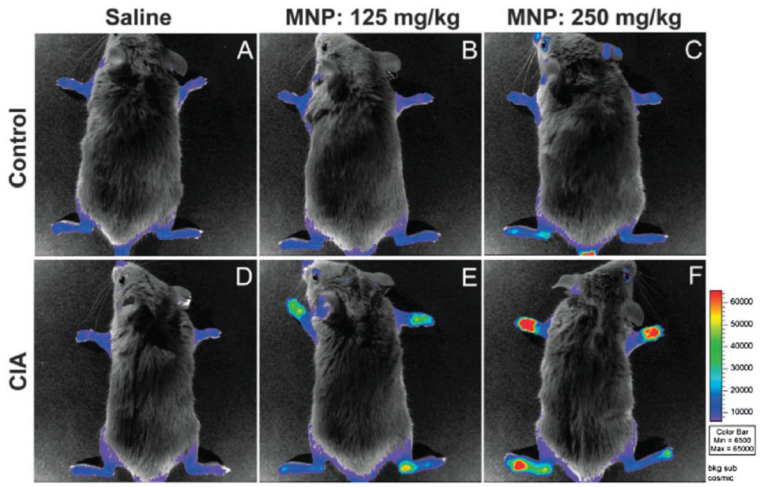

Fig. 8.

(Top) Control animals (without arthritis) that were intravenously-injected with two separate doses of (A) saline, (B) 125 mg SiNPs per kg, or (C) 250 mg SiNPs per kg 12 h before imaging. (Bottom) CIA animals with arthritis that were intravenously-injected with (D) saline, (E) 125 mg SiNPs per kg, or (F) 250 mg per kg. Reprinted from ref. 36 with permission from *Clinical and Experimental Rheumatology*.

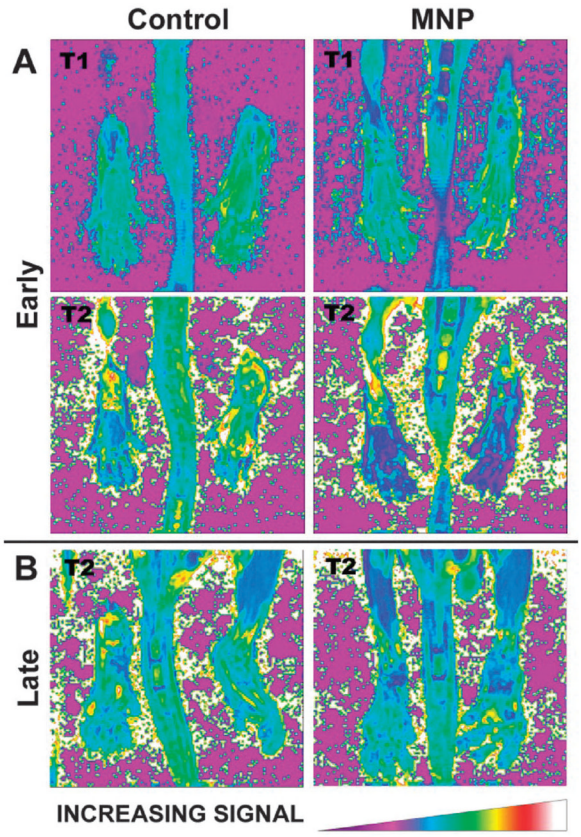

Fig. 9.

(A) Representative T_1 and T_2 relaxation maps of the hindlimbs of a mouse with early stage CIA before and after SiNPs administration. (B) T_2 relaxation maps of the hindlimbs of a mouse with later stage CIA before and after receiving a SiNP-based contrast agent. Reprinted from ref. 36 with permission from *Clinical and Experimental Rheumatology*.

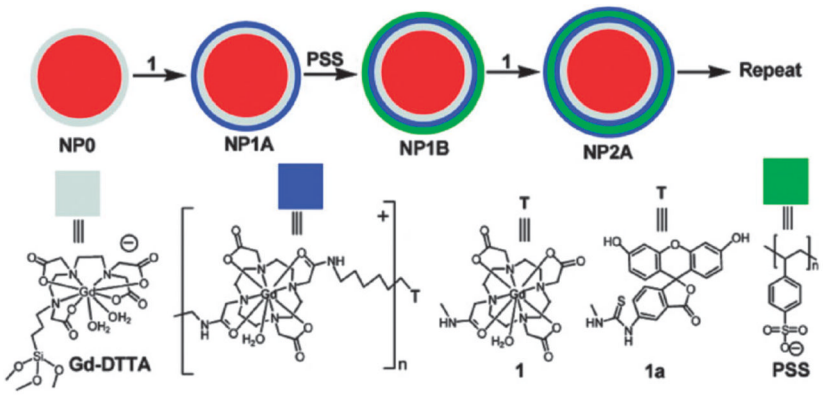

Fig. 10.
Schematic representation of the LbL self-assembly strategy for a dual optical and MR imaging multimodal contrast agent. Reprinted from ref. 37 with permission from American Chemical Society.

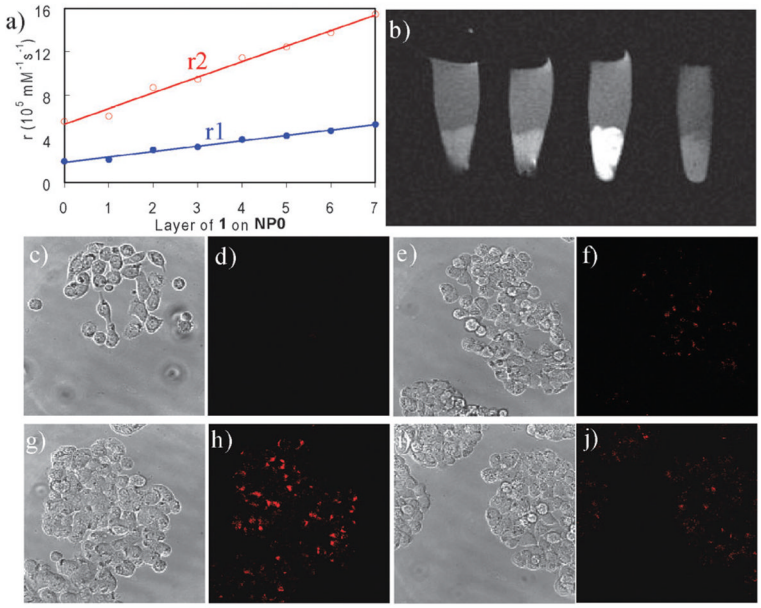

Fig. 11.

(a) Dependence of per particle r_1 and r_2 values on the number of deposited Gd–DOTA oligomer layers. (b) T_1-weighted MR images of HT-29 cells that have been incubated with various nanoparticles. From left to right: control cells without any nanoparticle, cells with LbL particles, cells with LbL particles that have been noncovalently functionalized with K7RGD, and cells with LbL particles that have been noncovalently functionalized with K_7GRD. Phase contrast optical (c, e, g, and i) and confocal microscopic images (d, f, h, and j) of HT-29 cells that have been incubated with various nanoparticles: control cells without any nanoparticle (c and d), cells with LbL particles (e and f), cells with LbL particles that have been noncovalently functionalized with K_7RGD (g and h), and cells with LbL particles that have been noncovalently functionalized with K_7GRD (i and j). Reprinted from ref. 37 with permission from American Chemical Society.

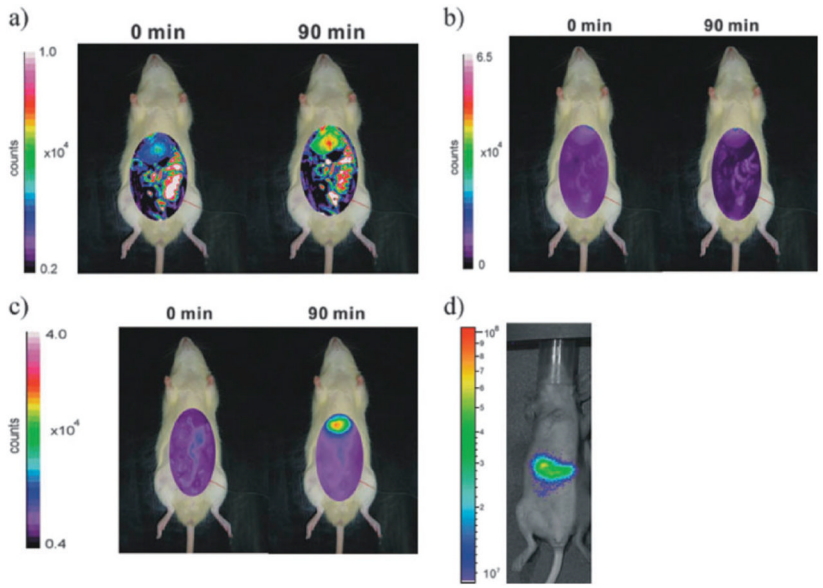

Fig. 12.

Biodistribution of FITC–MSNs in an anesthetized rat before and after (90 min) intravenous injection. The experimental conditions were set at 492 nm excitation and 518 nm emission and (a) a longer shutter time (60 s) for visible imaging and (b) a 30 s shutter time. (c) Biodistribution of ICG–MSNs in an anesthetized rat before and after intravenous injection for 90 min. The ICG–MSNs sample showed less interference from autofluorescence in a shorter shutter period (30 s). (d) ICG–MSNs in nude mice after intravenous injection for 3 h. Reprinted from ref. 44 with permission from John Wiley & Sons Inc.

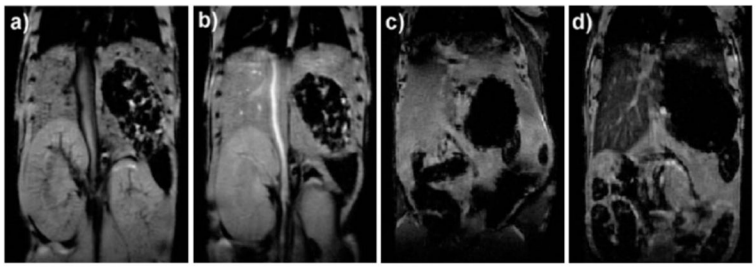

Fig. 13.

(a) Precontrast and (b) postcontrast (2.1 μmol kg^{-1} dose) T_1-weighted mouse MR image showing aorta signal enhancement. (c) Precontrast and (d) postcontrast (31 μmol kg^{-1} dose) mouse MR images showing liver signal loss due to T_2-weighted enhancement. Reprinted from ref. 46 with permission from American Chemical Society.

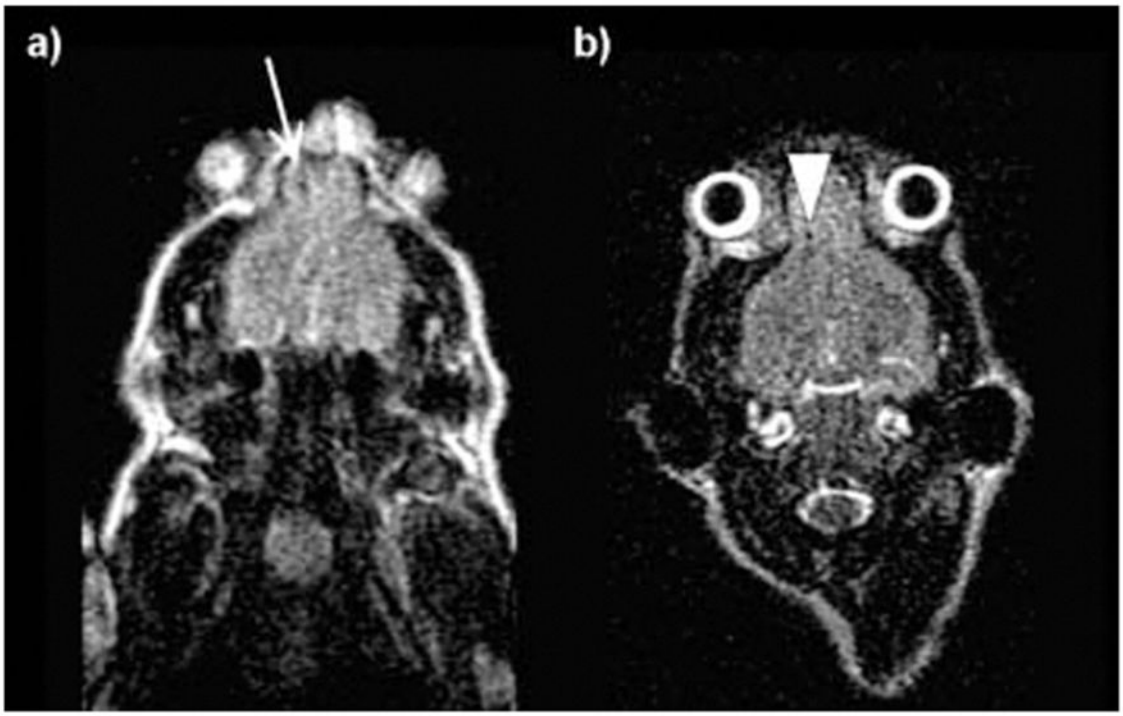

Fig. 14.

Clinical 1.5 T MR images of a nude mouse 8 h (a) and 9 days (b) after implantation of Mag-Dye@MSN-labeled hMSCs at the frontal cortex. (a) Using a clinical 1.5 T MR scanner, the hMSCs revealed a dark dot at the frontal cortex (arrow). (b) Repeated MR scanning was carried out 9 days after hMSC implantation. The stem cells could still be visualized as a black dot at the frontal cortex. No migration of these cells is found (arrow head). Reprinted from ref. 49 with permission from John Wiley & Sons Inc.

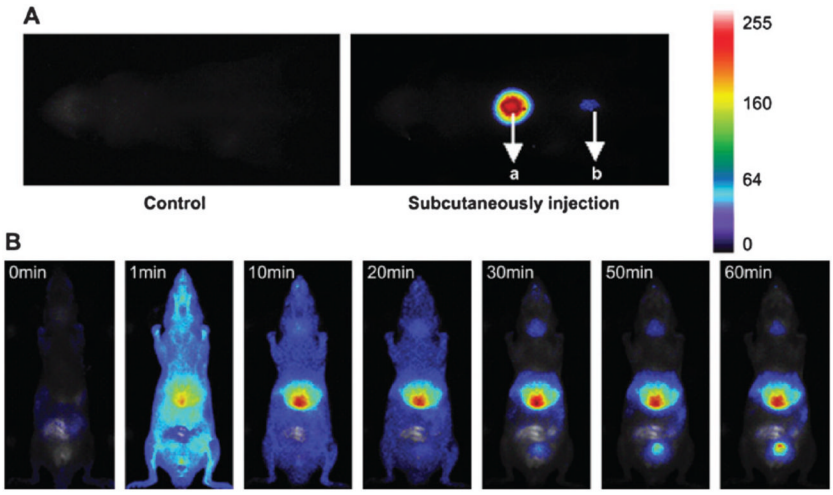

Fig. 15.

(A) Images of the two subcutaneous injections of 100 mL MB-encapsulated SiNPs with concentrations of 44 mg mL^{-1} (a) and 4.4 mg mL^{-1} (b). The acquisition was performed 2 min after injection. (B) Real-time *in vivo* abdomen imaging of an intravenous injection of 200 mL of MB-encapsulated SiNPs (44 mg mL^{-1}) at different time points, post-injection. Reprinted from ref. 53 with permission from Elsevier Ltd.

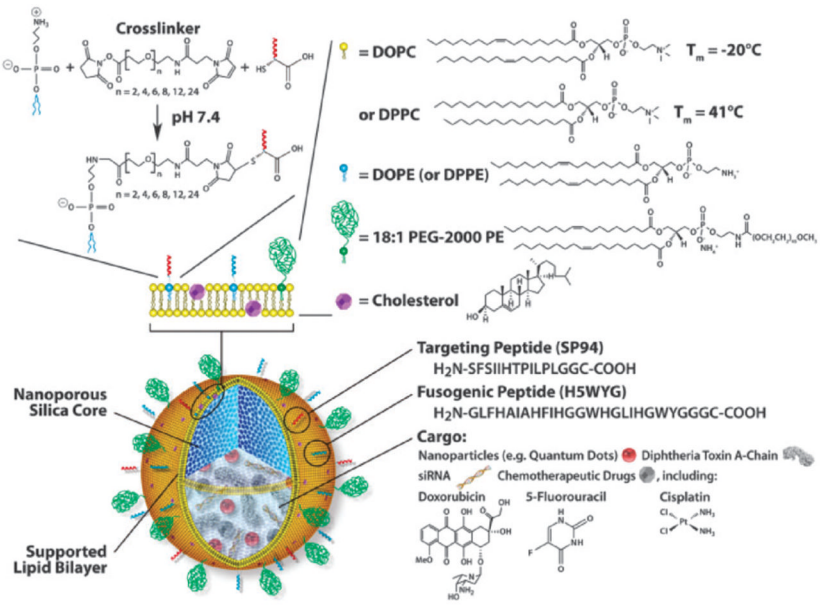

Fig. 16.

Schematic illustration of the nanoporous particle-supported lipid bilayer, depicting the disparate types of therapeutic and diagnostic agent that can be loaded within the nanoporous silica core, as well as the ligands that can be displayed on the surface of the SLB. Reprinted from ref. 57 with permission from Macmillan Publishers Ltd.

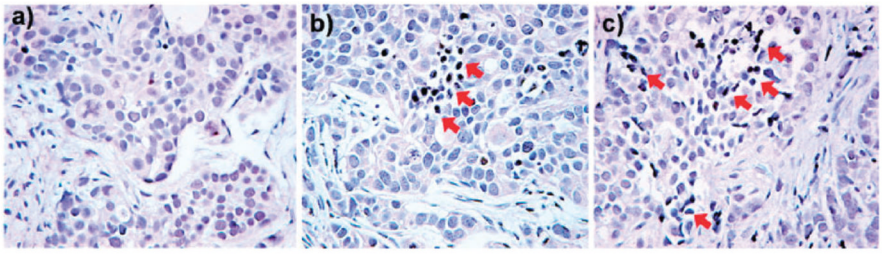

Fig. 17.

TUNEL assay for apoptotic cell death. Tumor section from a mouse that was given intravenous injection of (a) free IO-MSN, (b) DOX loaded IO-MSN (DOX 2 mg kg^{-1}), and (c) DOX loaded IO-MSN (DOX 4 mg kg^{-1}). Arrows indicate examples of TUNEL-positive (brown color) cells with apoptotic morphology. Reprinted from ref. 59 with permission from American Chemical Society.